Improving the Arterial Input Function in Dynamic Contrast Enhanced MRI by Fitting the Signal in the Complex Plane

Frank F.J. Simonis,[1]* Alessandro Sbrizzi,[2] Ellis Beld,[1] Jan J.W. Lagendijk,[1] and Cornelis A.T. van den Berg[1]

Purpose: Dynamic contrast enhanced (DCE) imaging is a widely used technique in oncologic imaging. An essential prerequisite for obtaining quantitative values from DCE-MRI is the determination of the arterial input function (AIF). However, it is very challenging to accurately estimate the AIF using MR. A comprehensive model, which uses complex data instead of either magnitude or phase, was developed to improve AIF estimation.

Theory and Methods: The model was first applied to simulated data. Subsequently, the accuracy of the estimated contrast agent concentration was validated in a phantom. Finally the method was applied to existing DCE scans of 13 prostate cancer patients.

Results: The complex signal method combines the complementary strengths of the magnitude and phase method, increasing the precision and accuracy of concentration estimation in simulated and phantom data. The in vivo AIFs show a good agreement between arterial voxels (standard deviation in the peak and tail equal 0.4 mM and 0.12 mM, respectively). Furthermore, the dynamic behavior closely followed the AIF obtained with DCE-CT in the same patients (mean correlation coefficient: 0.92).

Conclusion: By using the complex signal, the AIF estimation becomes more accurate and precise. This might enable patient specific AIFs, thereby improving the quantitative values obtained from DCE-MRI. **Magn Reson Med 76:1236–1245, 2016.** © **2015 Wiley Periodicals, Inc.**

Key words: DCE-MRI; arterial input function; complex signal; fitting

INTRODUCTION

In current clinical practice, dynamic contrast enhanced (DCE) imaging is widely used for oncologic imaging because it offers valuable information for diagnosis, treatment monitoring and response assessment (1,2). In longitudinal studies, DCE scans are subject to model fitting to obtain quantitative tissue perfusion related variables such as K^{trans} in the Tofts model (3). These quantitative values are in turn used for estimation of the severity of the disease, tumor volume delineation, and treatment response monitoring (4,5). However, large variations in K^{trans} can be found among studies, perfusion analysis solutions, and institutions, weakening its diagnostic and predictive value (6–8). An essential prerequisite for determining quantitative values from DCE-MRI is the absolute contrast agent (CA) concentration in the feeding arteries over time, referred to as the arterial input function (AIF). Various methods to determine the AIF have been published, ranging from measuring the temporal signal evolution inside feeding arteries or the aorta to indirect estimation from tissue enhancement curves (9–11). However, up to now no satisfactory solution has been proposed which can provide the required accuracy and robustness for patient specific AIFs. Therefore, most studies still use a population averaged AIF, ignoring intersubject variation (12).

The most common way of determining the AIF in DCE-MRI is based on measuring the temporal evolution of the signal magnitude inside a large feeding artery. MR signal magnitude is related to the CA concentration because the CA affects neighboring protons, shortening both T_1 and T_2*. By using a spoiled gradient echo (SPGR) sequence, highly T_1-weighted images can be made with a good spatiotemporal resolution (13). However, reconstructing CA concentration from the signal magnitude is challenging because their relationship is not linear and shows a saturation effect at high concentrations (14). Furthermore, the signal magnitude is influenced by other experimental phenomena such as partial volume effects, inflow effects and B_1 inhomogeneities, making correct concentration determination even more challenging (15,16).

To dispose of these adverse effects some years ago a method was proposed which uses the signal phase to determine the AIF (17,18). Signal phase changes due to the magnetic susceptibility of the CA. The main advantages of using signal phase are its linear relation to CA concentration and its insensitivity to inflow effects and B_1 inhomogeneities. However, using signal phase leads to other challenges. The phase is also affected by susceptibility changes in the proximity of the artery and magnetic field drift. To correct the phase after acquisition, efforts have been made to estimate the temporally varying magnetic fields within the arteries from neighboring voxels (6,19); however, problems remain. Another disadvantage of working with phase data is that its precision is much less at low CA concentrations. This is because the phase uncertainty then becomes much larger, because it

[1]Department of Radiotherapy, Imaging Division, University Medical Center Utrecht, Utrecht, the Netherlands.

[2]Department of Radiology, University Medical Center Utrecht, Utrecht, the Netherlands.

*Correspondence to: F.F.J. Simonis, M.Sc., Department of Radiotherapy, University Medical Center Utrecht, Heidelberglaan 100, 3584 CX, Utrecht, The Netherlands. E-mail: F.F.J.Simonis@umcutrecht.nl

Received 2 July 2015; revised 29 September 2015; accepted 30 September 2015

DOI 10.1002/mrm.26023

Published online 3 November 2015 in Wiley Online Library (wileyonlinelibrary.com).

scales inversely with the corresponding signal magnitude (20,21).

Recently it was pointed out that because magnitude and phase are governed by different CA dependent physical processes, a combination of both could be used to avoid shortcomings of using each method individually (22). In that research on simulated data, CA concentration was determined based on a maximum likelihood estimator combining signal phase and magnitude information. However, the phase and magnitude are also complementary. The saturation and nonlinear behavior of the magnitude signal mainly occurs at high concentrations, whereas signal phase inaccuracies are mostly present at low concentrations. The goal of this study was to develop a comprehensive model which uses complex data directly, instead of magnitude and phase separately, to exploit this complementary information. This can be achieved by fitting the enhancement data in the complex plane, as originally proposed to reduce partial volume effects in Dynamic Susceptibility Contrast MRI (23) and DCE-MRI (24). Here this method is applied to obtain a more accurate AIF. To keep the method practical, it was designed to require minimal user interaction, have a short computation time and perform in a robust manner. The comprehensive model was first tested on simulated data and compared with the magnitude-only and phase-only methods. Subsequently, the accuracy of the estimated CA concentration was validated in a phantom study. Finally the method was applied to DCE scans of prostate cancer patients and compared with DCE-CT results of the same patients.

THEORY

A comprehensive model was developed to fit the DCE signal in the complex plane. For this purpose two separate models were combined: a model for signal magnitude change due to the changing relaxation times and a model of signal phase change caused by magnetic field distortion due to a susceptibility distribution.

Magnitude-Only Method

Signal magnitude is determined by both the pulse sequence and the CA concentration. A short repetition time (TR), spoiled gradient echo is most commonly used in DCE-MRI, because of its high attainable temporal resolution while maintaining good 3D coverage. The signal magnitude at steady state of this sequence is defined as (25):

$$|S| = \rho_{eff}\frac{\sin(\alpha)\left(1-e^{-\frac{TR}{T_1(C)}}\right)}{1-\cos(\alpha)e^{-\frac{TR}{T_1(C)}}}e^{-\frac{TE}{T_2^*(C)}} \quad [1]$$

where $|S|$ is the signal magnitude for a given spatial location and a given time, α is the flip angle, TE is the echo time and ρ_{eff} is the spin density including system gain contributions. C is the time dependent CA concentration, which needs to be estimated for the whole exam duration. In the fast exchange limit which is usually assumed in DCE-MRI, the dependency of T_1 and T_2^* on C is known (26):

$$\frac{1}{T_1(C)} = \frac{1}{T_{10}} + r_1 C \quad [2]$$

$$\frac{1}{T_2^*(C)} = \frac{1}{T_{20}^*} + r_2^* C \quad [3]$$

with T_{10} and T_{20}^* being the T_1 and T_2^* of the voxel before contrast injection, and r_1 and r_2^* the longitudinal and transverse relaxivities of the CA. Some variables are set on the scanner (α, TE, and TR), and some are known from literature (r_1, r_2^*). However, ρ_{eff}, T_{10}, and T_{20}^* are not known before the measurement. There are several methods to estimate these unknowns from tissues by doing several so called prescans with varying flip angles (27). However, AIF determination is a specific case because the T_{10} and T_{20}^* of blood are known. Then the relative signal enhancement can be used, such that ρ_{eff} drops out of the equation (14):

$$\frac{|S|-|S_0|}{|S_0|} = \frac{\left(e^{-\frac{TR}{T_1(C)}}-1\right)\left(\cos(\alpha)e^{-\frac{TR}{T_{10}}}-1\right)}{\left(e^{-\frac{TR}{T_{10}}}-1\right)\left(\cos(\alpha)e^{-\frac{TR}{T_1(C)}}-1\right)}\left(\frac{e^{-\frac{TE}{T_2^*(C)}}}{e^{-\frac{TE}{T_{20}^*}}}\right)-1 \quad [4]$$

in which S_0 is the baseline signal that is measured before CA injection. Because all variables except C are known, a CA concentration estimate can be found for each signal time point individually. This function, however, has a maximum detectable concentration, defined as the point where the signal magnitude is maximal (14). At higher CA concentrations, the magnitude decreases due to T_2^* effects, resulting in two solutions, making it impossible to discriminate higher concentrations from lower values.

Phase-Only Method

Another method of estimating the CA concentration uses the signal phase. However, phase changes are caused by susceptibility changes that depend on all surroundings. This results in interconnected and spatially dependent equations. Therefore, a simplification has to be made for the geometry, enabling an analytical solution. The femoral arteries, often used for determining the AIF in DCE exams of the prostate, can be represented fairly accurately as infinitely long cylinders parallel to the main magnetic field (23). The phase inside such a cylinder with a CA dependent susceptibility can then be described by:

$$\theta(C) = \theta_0 + {}^1\!/_3\omega_0 TE\ \chi_m C \quad [5]$$

where θ_0 is the initial phase, ω_0 the resonance frequency of protons, TE the echo time, χ_m the molar susceptibility of the CA and C the concentration of the CA. Similar to the signal magnitude method a baseline estimation needs to be done, in this case to determine θ_0. When θ_0 is known, the concentration at each individual time point directly follows from the phase.

Complex Signal Fitting Method

Combining both models results in the following equation for the complex signal dependence on CA concentration:

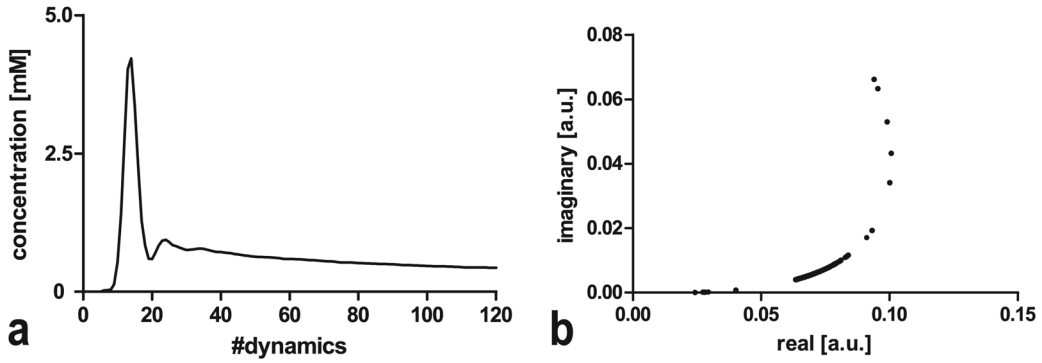

FIG. 1. **a**: A synthetic AIF. **b**: The resulting trajectory in the complex plane.

$$S = \tilde{\rho}_{\text{eff}} \frac{\sin(\alpha)\left(1 - e^{-\frac{TR}{T_1(C)}}\right)}{1 - \cos(\alpha)e^{-\frac{TR}{T_1(C)}}} e^{-\frac{TE}{T_2^*(C)}} \cdot e^{-i\theta(C)} \quad [6]$$

in which $\tilde{\rho}_{\text{eff}}$ is defined as a complex number: $\tilde{\rho}_{\text{eff}} = \rho_{\text{eff}} \cdot e^{-i\theta_0}$. During an experiment, the CA concentration varies, making C to actually be an array $\vec{\mathbf{c}}$ containing all concentrations in time. Because both phase and magnitude are used in this method the number of data points is twice the number of concentrations, enabling a fit of the complete array $\vec{\mathbf{c}}$ instead of a point-wise estimation of each individual concentration. Because each voxel shares the same time independent $\tilde{\rho}_{\text{eff}}$ and α, these quantities can be simultaneously fit with all concentrations instead of estimated solely from baseline images.

AIF Estimation

The complex signal model should be fit to the signal of a voxel over time to obtain an AIF. An example of the complex signal evolution of an AIF can be seen in Figure 1, in which the peak of the AIF is the outermost point. The points in the tail of the AIF are clustered together on this curve, because they share an almost equal concentration. However, not all signal data are equally reliable. The magnetic field usually drifts over time and changes with the amount of CA present in the tissue (28), so the phase of later time points is less reliable. The result of a magnetic field drift that increases linearly over time results in a clear deviation in the phase of later time points as shown in Figure 2a. However, the method can be adjusted to mitigate the errors due to these affected points. Usually the fitting is done using a non-linear least square fit:

$$(\tilde{\rho}_{\text{eff}}, \alpha, \vec{\mathbf{c}}) = \arg \min_{(\tilde{\rho}_{\text{eff}}, \alpha, \vec{\mathbf{c}})} \|\boldsymbol{f}(\tilde{\rho}_{\text{eff}}, \alpha, \vec{\mathbf{c}}) - \hat{\boldsymbol{s}}\|^2 \quad [7]$$

in which $\hat{\boldsymbol{s}}$ is the measured data and $\vec{\mathbf{c}}$ the resulting fit concentration. Because later time points are more prone to drift, the fit can be adjusted to discard those points. In this case a weighted least squares fit can be solved:

$$(\tilde{\rho}_{\text{eff}}, \alpha, \vec{\mathbf{c}}) = \arg \min_{(\tilde{\rho}_{\text{eff}}, \alpha, \vec{\mathbf{c}})} \|\boldsymbol{W}(\boldsymbol{f}(\tilde{\rho}_{\text{eff}}, \alpha, \vec{\mathbf{c}}) - \hat{\boldsymbol{s}})\|^2 \quad [8]$$

with $\boldsymbol{W}$ being a diagonal matrix containing the weights of each time point. When the weights in the tail of the AIF are negligibly small compared with the earlier time points, they no longer influence the fit of $\tilde{\rho}_{\text{eff}}$ and α which determine the curve shape. This improves all concentration estimations, see Figure 2b.

METHODS

Numerical Simulations

Numerical simulations were performed to compare the AIF estimation of the proposed complex signal method with the magnitude-only and phase-only method. A complex signal produced by a steady baseline (10 points, 0 mM) followed by a linearly increasing concentration of gadobutrol (0–8.5 mM, $\chi_m = 320$ ppm, $r_1 = 3.6$ L/mmol/s,

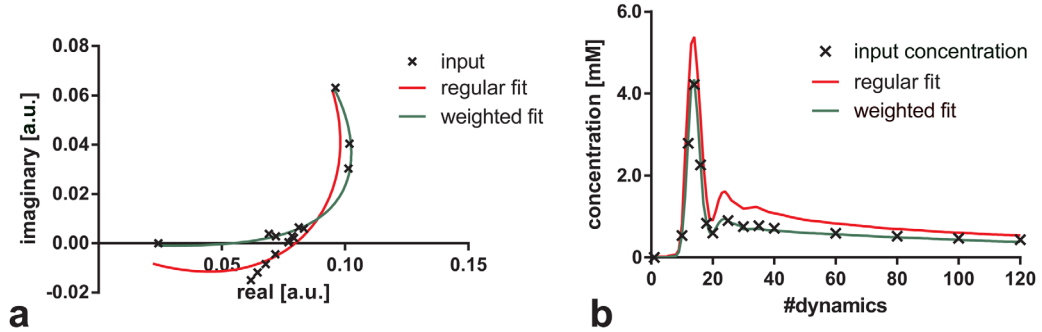

FIG. 2. **a**: The complex trajectory described by an AIF with added linear drift (black). This was used as the input for a regular and a weighted non-linear least squares fit. **b**: The resulting concentration from both fits compared with the input concentration.

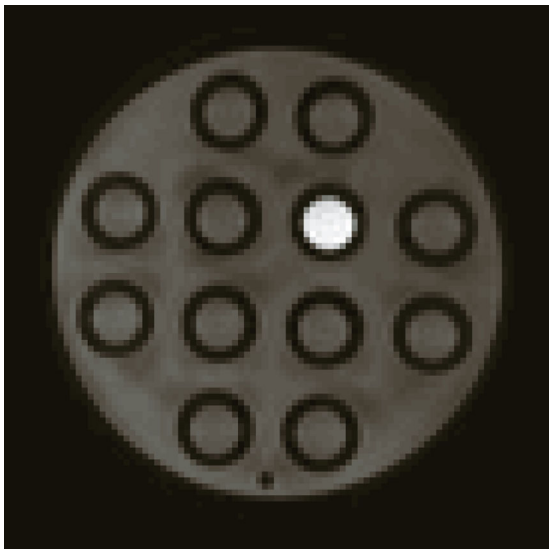

FIG. 3. Magnitude image of a transverse slice of the water-filled phantom containing 12 test tubes. The bright tube contains 0.5 mM gadobutrol.

and $r_2^* = 6.3$ L/mmol/s) (6,29) was simulated based on Eq. [6], with the scan parameters of the clinical DCE sequence at our institute (flip angle 8°, TE/TR 1.7/4 ms) (6). Subsequently, Gaussian noise was added such that the signal-to-noise ratio (SNR) had a realistic value compared with in vivo scans. The mean of the signal divided by the standard deviation of the noise equaled 13. The T_1 and T_2^* of blood were set to literature values at 3 tesla (T) (1.932 and 0.275 s, respectively) (30). The CA concentration was estimated from the magnitude using Eq. [4], in which S_0 was defined as the mean magnitude of the baseline points. Each concentration was found by minimizing the norm of the difference between the simulated data and the estimates. The phase data resulted in concentrations by means of Eq. [5], in which θ_0 was defined as the mean phase of the baseline points. The complex signal method was finally applied to the complex signal. In the fitting procedure, the initial estimations were set as follows: the initial flip angle was set to the input angle, with lower and upper boundaries set to 2° and 20°, respectively, the initial concentrations were set to zero with an upper bound of 10 mM and a lower bound of −0.1 mM. The lower boundary was set a little below zero to be able to cope with noise effects at low concentrations. The simulation described above was repeated a thousand times with different noise to quantify the precision and accuracy of each individual method. All fitting, data analysis, and post-processing were done in Matlab (The MathWorks Inc., Natick, MA).

Phantom Experiment

Phantom imaging was performed on a 3T MR scanner (Ingenia, Philips Healthcare, Best, The Netherlands). A plastic cylinder filled with tap water (height 6.5 cm, radius 10 cm) was used as a phantom. This phantom contains twelve cylindrical openings that can be filled with test tubes (height 7.5 cm, radius 1 cm). Test tubes with known concentrations of gadobutrol (0, 0.5, 1.5, and 10 mM dilutions of Gadovist, Schering, AG, Berlin, Germany) in tap water (T_{10}/T_{20}^* set to 2.5/0.5 s) were placed consecutively in the same center opening simulating an artery. Test tubes filled only with tap water were placed in all other openings. A transverse image of the phantom can be seen in Figure 3. This phantom was placed inside a head coil (dStream HeadSpine coil, Philips Healthcare, Best, The Netherlands). All five test tubes were scanned in order of increasing CA concentration while keeping the B_0 field shim settings constant. The scan on the test tube without CA was repeated as a final sixth scan. The DCE-MRI exam that was performed was equal to the clinical protocol. It consisted of a T_1-weighted 3D spoiled gradient echo sequence (20 transverse slices, slice thickness 5.0 mm, TE/TR 1.7/4.0 ms, acquisition matrix 160 × 160, SENSE 2, FOV 40 cm, flip angle 8°). A total of 120 dynamics were obtained at a 2.4 s time interval. The large amount of dynamics were scanned to determine the influence of magnetic field drift.

Because six experiments were done, each with their own resonance frequency calibration, all signals were corrected by using a reference region of interest in the phantom which was not affected by the CA. To make sure the signal was in steady state as described by the models, the first dynamic scan of each series was removed. Twenty-five voxels within the test tube in a center slice were manually selected and their concentrations were estimated to determine the accuracy and precision. The baseline signal which is required for the magnitude and phase method was set to the mean signal over 10 dynamic scans of the test tube without CA. For the complex signal fitting procedure, the initial values were as follows: the initial flip angle was set to 8° and restricted to realistic experimental values (between 6 and 10°), all initial concentrations were set to zero, with a lower boundary of −0.1 mM and an upper boundary of 15 mM. To minimize the influence of magnetic field drift on the complex signal fit, only the first dynamic scans of each test tube were included in the fit. This was done by reducing the weights of the other dynamic scans until they no longer significantly affected the fit.

In Vivo Experiment

Finally, the method was tested on DCE-MRI data acquired at 3T from 13 prostate cancer patients from an earlier conducted IRB approved study using the same scan sequence (6). A Regional Saturation Technique (REST) slab was placed 4 cm superior to the imaging region with a flip angle of 110 degrees to reduce the inflow effects (31). In each patient 0.1 mL/kg gadobutrol (1.0 M Gadovist, Schering AG, Berlin, Germany) was injected with a power injector (1 mL/s or 2 mL/s), followed by a saline flush. AIFs obtained from CT scans (AIF_{CT}) in the same patients, a median of 8.5 days apart from the DCE-MRI were used as a golden standard. The injection of the iodine contrast agent (Ultravist 300, Schering AG, Berlin, Germany) was done with a power injector (60 mL, 6 mL/s) followed by a saline flush (6). For the analysis, both femoral arteries were manually

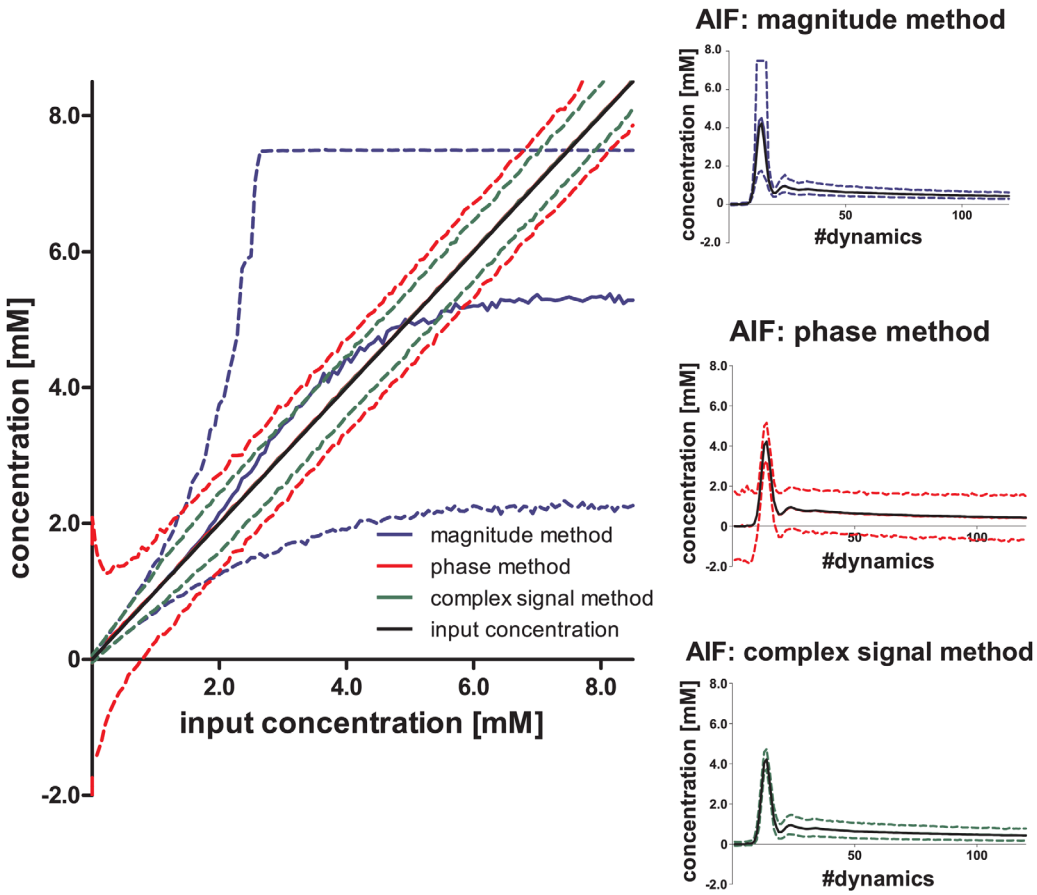

FIG. 4. Mean concentrations that were fit from simulated MR signals based on a ground truth input concentration (black) with flip angle 8°, TE = 1.7 ms, TR = 4 ms and realistic noise using the magnitude (blue), phase (red) and complex signal (green) method. The dashed lines show the lower 5% and upper 95% boundaries. In the left graph the results are presented for a linear input, the right graphs portray the results with a simulated AIF as input. The boundaries are equal for identical input concentrations. The magnitude method mainly fails at high concentrations whereas the phase method has problems estimating the lower concentrations. The complex fit method has a high precision over all concentrations.

delineated in 3 transverse slices in which the arteries were almost parallel to the main magnetic field. All voxels within the delineation with a cumulative intensity higher than 90% of the maximum cumulative intensity of the slice were selected. The AIF was determined for each voxel individually and subsequently the mean value of all voxels was calculated. The same boundaries as used for the simulated data were applied. The initial values were also kept equal except for the concentration which was set to 1 mM which is a rough estimation of the mean value of an AIF. Because the points in the tail of the AIF (all points later than the 30^{th} dynamic scan) are more prone to magnetic field drift they were excluded from the fit, i.e., their weights in the fit were reduced so they no longer affected the fit of $\tilde{\rho}_{eff}$ and α. Another reason for this is that the sampling density over all concentrations is much higher at the tail of the AIF. If the weights would not be reduced, the tail would have a disproportionately large influence on the curve shape. To compare the results with the AIF_{CT}, the concentrations were normalized to injected dose (6). The Pearson's correlation coefficient between the two AIFs was determined by dividing their covariance with the product of their individual standard deviations. This was used as a quantitative measure for the similarity in curve shape.

RESULTS

Numerical Simulations

The accuracy of using the phase-only, the magnitude-only and the complex signal method for concentration determination was examined using numerical simulations. The results can be seen in Figure 4, which shows the mean value of all three methods and their 90% confidence interval. The results of the magnitude method show high accuracy at low concentrations but the errors rapidly increase to intolerable values (>100% of the actual concentration) at higher concentrations. At a concentration of 7.5 mM, the fit on magnitude data even clips, because it is unable to detect higher values. The signal phase method clearly outperforms the magnitude method at high concentrations. However, at lower concentrations, i.e., low signal magnitude, errors are more pronounced in the phase. Because the baseline and the complete tail of the AIF will be around 0–2 mM of CA, this will have a big impact on AIF estimation, depicted in the right graphs of Figure 4. The complex signal method

Table 1
Root-Mean-Square Error of Concentrations in Range of the Tail of the AIF (0-2 mM) and the Peak of the AIF (4-5 mM) for Simulated Data at a Realistic SNR and for Phantom Data

		RMSE tail [mM]	RMSE peak [mM]
Simulated data	Magnitude-only	0.13	2.08
	Phase-only	0.61	0.49
	Complex signal	0.18	0.28
Phantom data	Magnitude-only	0.14	2.03
	Phase-only	0.48	0.30
	Complex signal	0.18	0.28

has a high precision and accuracy over the complete range of concentrations. The root-mean-square errors (RMSE) of concentrations at the tail and peak of the AIF are mentioned in the top rows of Table 1.

Phantom Experiment

Subsequently, the methods were tested on a phantom with known CA concentrations. Because each test tube was scanned for 120 dynamics this experiment also offered the possibility to illustrate the effect of magnetic field drift on concentration estimation. The drift caused a linearly increasing phase up to 0.1 radians over 120 dynamics (5 min of scanning) and was roughly equal for all scans. A weighted fit was performed on the complex signal, minimizing the influence of dynamics which are influenced by magnetic field drift, see Figure 5. The sensitivity and accuracy of the methods were tested by estimating the concentration from all dynamics of 25 voxels, the result of which can be seen in Figure 6. The resulting RMSE values are mentioned in the bottom rows of Table 1. The magnitude method again was unable to estimate values above its maximal detectable concentration but detected the lower concentrations with a high accuracy (RMSE = 0.14 mM). The magnitude method is unaffected by magnetic field drift because it only changes signal phase, therefore, the concentration estimation does not vary over the dynamics. However, the influence of drift on the phase-only method is clearly visible in Figure 6.

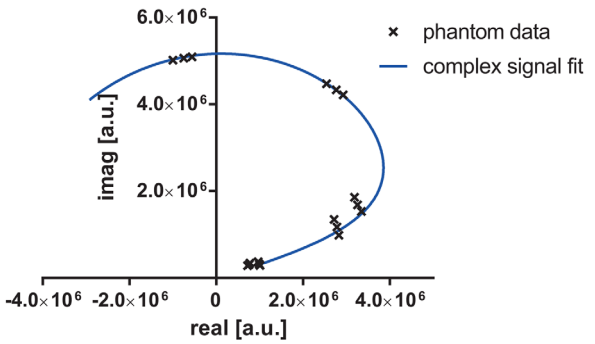

FIG. 5. An example of a weighted fit on complex phantom data from the first, middle, and final dynamic scan of one voxel, showing a curved trajectory with increasing concentration. The curve fit is determined by the first dynamic scans. The B_0 drift corresponds to a rotation around the origin causing the signal to shift perpendicular to the curve for low concentrations but tangential to the curve for higher concentrations.

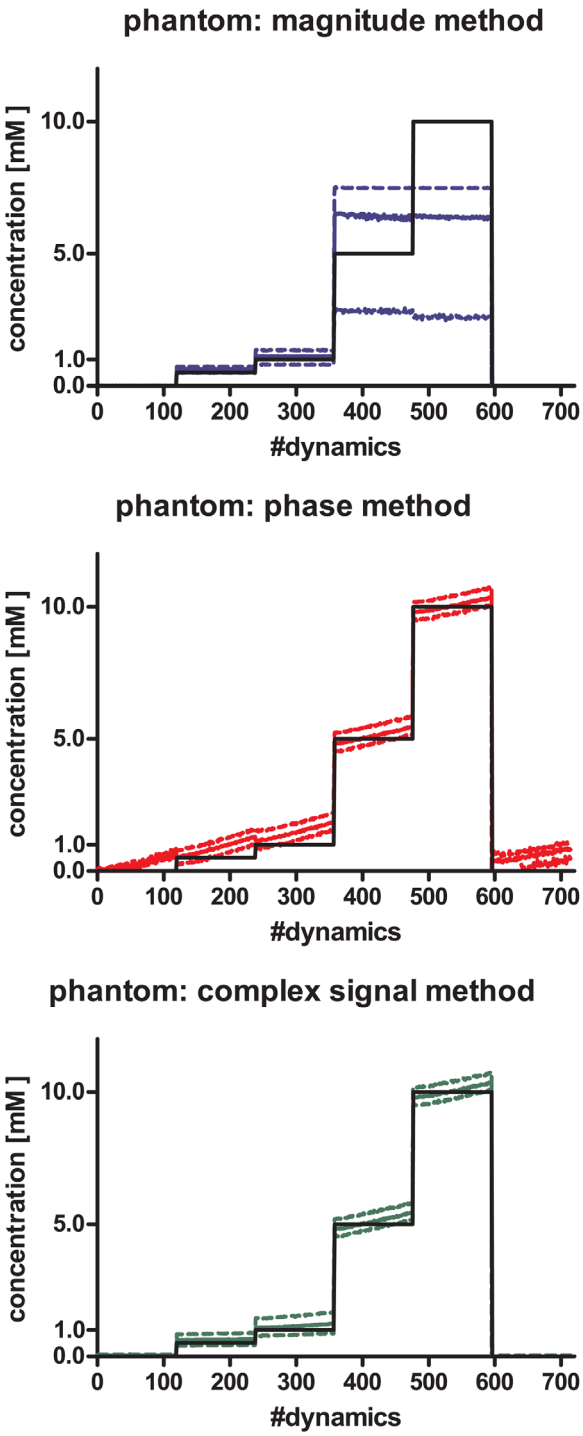

FIG. 6. Estimated mean CA concentrations in the phantom using the magnitude, phase, and complex signal method compared with the true concentration (black). The dashed lines show the lower 5% and upper 95% boundaries.

The estimated concentration increases with every dynamic due to drift, increasing the error. The fit concentrations from the complex signal method follow the magnitude method at low concentrations and agree with the phase method at high concentrations combining the strengths of both methods. The mean estimated flip angle was 8.1°, which is in accordance with the value of 8° that was set on the scanner.

In Vivo Application

All methods were also tested on purely arterial voxels of prostate cancer patients. Because no true concentrations were known for these patients, the AIFs obtained by CT were used as a gold standard. The results of fitting all voxels of the left and right femoral artery of a single patient can be seen in Figure 7. The magnitude-only method clearly underestimated the CA concentration compared with the AIF_{CT}. So although all voxels give similar results, the peak is hardly discernable making all AIFs obtained by the magnitude-only method inaccurate. The phase-only method performed better with a mean AIF that is similar to the AIF_{CT}. However, there is considerable variation between voxels and negative concentrations are estimated. The results from the complex signal fit show the least amount of variation between voxels and the highest correlation with AIF_{CT}. All methods were also applied to the other 12 patients. In Figure 8, the mean and spread (5% and 95% boundary) of the AIFs determined from all voxels with the complex method are shown together with the $AIF_{CT.}$ These AIFs not only show a clear first pass peak but a second pass can also be observed in some patients. Quantitative values describing the standard deviation between voxels and correlation with AIF_{CT} can be found in Table 2. All patients show a small spread in the individual voxels and each correlation coefficient with AIF_{CT} is higher than those obtained with the signal magnitude and phase methods. The lowest correlation coefficient equaled 0.84 and was caused by a low amount of arterial voxels and low SNR in that specific patient. The mean estimated flip angle was unrealistically low compared with the value set on the scanner with a value of $3.6 \pm 1.0°$ for the left and $2.9 \pm 0.8°$ for the right artery.

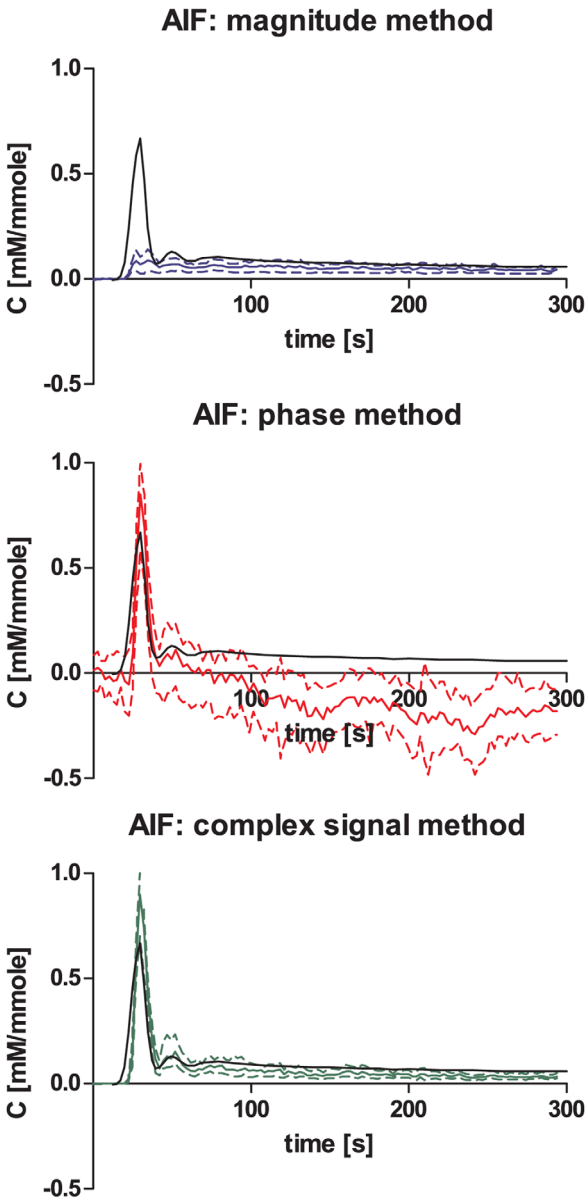

FIG. 7. Estimated mean normalized AIFs using the magnitude, phase and complex signal method compared with the AIF measured by DCE-CT (black). The data were normalized to the dose to compare CT and MR. The dashed lines show the lower 5% and upper 95% boundaries. The data was fit on 48 voxels within the arteries from 3 slices of a single patient.

DISCUSSION

Numerical Simulations

The goal of this research was to improve the determination of CA concentration for correct estimation of the AIF in DCE-MRI. First a comparison between existing methods and the complex signal method was made using simulated data. The magnitude-only method led to large errors, especially at high concentrations. The mean value of all concentration estimations is also incorrect, thus averaging over multiple voxels would not improve the method. An intrinsic difficulty is the accurate estimation of S_0 because large errors occur in the estimated concentrations when this is incorrectly determined. This requires either a high SNR in the baseline measurements or a high number of baseline samples. Furthermore, there is a maximum concentration that can be detected. Although this maximal value can be increased by using a higher flip angle (14), this would in turn worsen S_0 determination. Furthermore, higher flip angles could lead to lower achievable temporal resolution as the global SAR limit becomes a constraining factor. The signal magnitude is also sensitive to experimental imperfections such as incorrect flip angles and inflow effects, significantly deteriorating the concentration estimation, which were not taken into account in the numerical simulations. When the simulated DCE signal phase is used no saturation occurs and the optimal flip angle is simply the Ernst angle which results in highest signal-to-noise and phase accuracy. However, the challenge of determining a correct baseline signal (in this case θ_0) remains. The standard deviation of the signal phase is inversely proportional to its magnitude (20), leading to much lower precision at low magnitudes, i.e., low concentrations. This made it challenging to obtain a correct estimate for θ_0 which determines the phase value at C=0. If the value of θ_0 is incorrect, the whole concentration curve will be affected.

Similar to the magnitude-only method, the phase-only method would benefit from using more baseline measurements to achieve a more accurate baseline estimation.

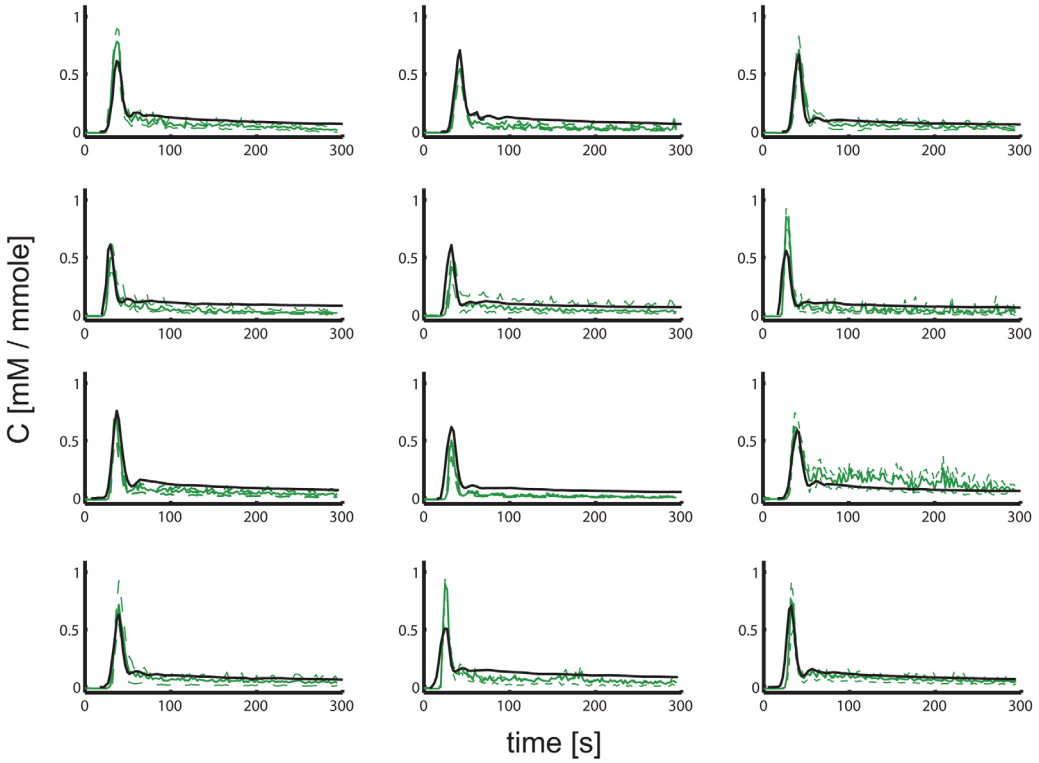

FIG. 8. Mean normalized AIFs estimated by the complex signal method on 12 patients compared with the AIFs obtained with DCE-CT. The dashed lines show the lower 5% and upper 95% boundaries

The complex signal fitting method takes a completely different approach, because it relies on the fact that all points of the simulated DCE signal can be fit onto a single curve. This enables the estimation of $\tilde{\rho}_{\text{eff}}$ and α from all time points instead of just the baseline measurements. Furthermore, the concentrations are then determined based on the complementary information of magnitude and phase. Out of the three tested methods the complex method had the most constant concentration estimation for the simulated data, combining a high accuracy with a high precision over the complete dynamic range.

Phantom Experiment

To quantify how the methods perform in practice, they were tested on a phantom with known concentrations of CA. The phantom experiments show that the complex signal method is able to correctly determine concentrations of gadobutrol within the clinical range with a minimal error (RMSE equals 0.18 and 0.28 mM at the tail and the peak of the AIF, respectively). Also the flip angle was correctly estimated. The analysis of the phantom experiments demonstrates that the error in concentration estimation caused by magnetic field drift depends on the CA concentration. At low concentrations, the phase change due to drift shifts the signal perpendicular to the curve described by an increasing concentration, see Figure 5. This did not affect the concentration estimation in the complex signal method, which can be seen in Figure 6. At higher concentrations, magnetic field drift results in a tangential shift, because the magnitude almost stays constant as the concentration changes and the shape of the curve approaches a circle. This causes phase effects to resemble an increase in concentration, causing a drift dependent error. Because in an in vivo situation drift will mainly occur at the tail of the AIF, i.e., at low CA concentrations, drift will have a small effect on concentration estimation in practice. The specific amount of magnetic field drift however depends on the gradient coil usage, vendor specific hardware design, and software tools.

Table 2
Correlation between the Mean AIF, Obtained from Different Voxels Using the Three Methods, and the AIF Obtained from DCE-CT[a]

	Correlation with AIF_{CT}	SD peak [mM]	SD tail [mM]
Magnitude-only	0.50	0.16	0.08
Phase-only	0.87	0.67	0.5
Complex signal	0.92	0.43	0.12

[a]The second and third column show the mean standard deviation of all voxels at the peak and the tail of the AIFs .

In Vivo Application

The concentration estimations based on in vivo data were compared with AIFs obtained in the same patient by DCE-CT. Not only did the use of the comprehensive complex model result in less variation in AIFs of separate voxels, it also improved the correlation with AIF_{CT} compared with the methods based on magnitude or phase only.

One of the challenges that occurs in vivo is an inhomogeneous B_1 field, leading to varying flip angles for different voxels. An advantage of having the flip angle α as a variable in the fit is that the method is able to compensate for this. However, the flip angle that was found (around 3° instead of 8° set on the scanner) is too low to be caused by a change in the B_1-field. Because the flip angle was correctly estimated in the phantom experiment, the underestimation in the in vivo data was most likely caused by inflow effects, i.e., an increased signal due to inflowing blood which has a higher magnetization because it received less RF pulses, despite the use of a REST slab. Inflow effects lead to higher signal magnitudes than described by the model, mainly at low CA concentrations. The magnitude model, therefore, overestimates S_0, leading to an underestimation of all subsequent concentration values. The complex model still fits accurately to the data albeit with a lower flip angle and higher $\tilde{\rho}_{eff}$ then normal. Because signal phase is unaffected by inflow effects, the errors were much less pronounced in the complex signal method than in the magnitude method.

An experimental phenomenon which was not taken into account in the complex signal model is the partial volume effect, i.e., signal of neighboring tissue interfering with the arterial signal in a voxel. This would lead to a portion of the signal being dependent on the CA concentration in another way than the model describes. As a result, the change of both signal magnitude and phase due to CA alters, leading to AIF misestimation. Possible solutions to this problem have already been proposed for the complex signal method (23,24). However, in this research, a large artery was used for analysis (7–10 mm diameter) and the images consisted of a voxel size of 0.8 mm^2. Therefore, partial volume effects only occurred at edge voxels which were not included in AIF estimation.

Another source of error comes from using standard literature values for T_{10} and T^*_{20} in the model. A misestimation in T^*_{20} has a negligible effect due to the fact that T^*_2-effects are minimal with in vivo concentrations in DCE-MRI, but the T_{10} does influence the concentration estimation. In this research the literature value of (29) was used, but other studies report lower values for the T_1 of blood, sometimes even incorporating hematocrit and oxygenation level for more precision (32–34). In our method, the impact of reported differences in T_{10} was relatively small (< 0.3 mM). However, other values can easily be used in the model and would only influence the magnitude part of the model.

The complex signal method does not put any extra restrictions on a regular clinical DCE sequence except that full complex data needs to be saved, which takes no extra scan time. This enables retrospective application of the method, provided complex data is available. Furthermore, the method is almost fully automatic and manual interaction is only required for delineation of the arteries. The fitting procedure takes on average 2.8 s per voxel and is numerically stable, so the analysis on one patient takes roughly 1.5 min. Because the method is more precise than magnitude or phase methods, it might enable patient specific AIFs from DCE-MRI. This might be valuable for future research because K^{trans} and v_p of the pharmacokinetic model used for DCE data (3) are highly dependent on a correct peak concentration of the AIF (35). This peak concentration is notoriously difficult for the commonly used magnitude-only method. Therefore, improvements are expected but the exact effect on the precision of DCE parameters should be subject to further investigations.

The complex signal fitting could in theory also be applied for concentration estimation in tissue instead of inside arteries. This does require additional adjustments. First, because T_{10} and T^*_{20} are no longer known, they should be measured in prescans. Furthermore, a description for the phase which is not dependent on geometry, such as proposed by Brynolfsson et al (22), should then be used.

CONCLUSIONS

The CA concentration within arteries can be measured more accurately when using the complex signal of the DCE-MRI. By using the complementary information of phase and magnitude, the arterial input function estimation becomes more accurate and precise. The method can also be adjusted to cope with experimental phenomena such as magnetic field drift. By improving the measurement of CA concentration a patient specific arterial input function might become possible, thereby improving the quantitative models that rely on it.

ACKNOWLEDGMENTS

This research is fully funded by ZonMw Electromagnetic Fields & Health program “Measuring EMF induced tissue heating and physiological changes in-vivo” (85300005).

REFERENCES

1. Padhani AR. Dynamic contrast-enhanced MRI in clinical oncology: current status and future directions. J Magn Reson Imaging 2002;16: 407–422.
2. Jackson A, Buckley DL, Parker GJM, editors. Dynamic contrast-enhanced magnetic resonance imaging in oncology. Berlin: Springer; 2005.
3. Tofts PS, Brix G, Buckley DL, et al. Estimating kinetic parameters from dynamic contrast-enhanced T1- weighted MRI of a diffusable tracer: standardized quantities and symbols. J Magn Reson Imaging 1999;10:223–232.
4. Haider MA, Chung P, Sweet J, Toi A, Jhaveri K, Ménard C, Warde P, Trachtenberg J, Lockwood G, Milosevic M. Dynamic contrast-enhanced magnetic resonance imaging for localization of recurrent prostate cancer after external beam radiotherapy. Int J Radiat Oncol Biol Phys 2008;70:425–430.
5. Moman MR, van den Berg CAT, Boeken Kruger AE, Battermann JJ, Moerland MA, van der Heide UA, van Vulpen M. Focal salvage guided by T2-weighted and dynamic contrast-enhanced magnetic resonance imaging for prostate cancer recurrences. Int J Radiat Oncol Biol Phys 2010;76:741–746.
6. Korporaal JG, Van Den Berg CAT, Van Osch MJP, Groenendaal G, Van Vulpen M, Van Der Heide UA. Phase-based arterial input function measurements in the femoral arteries for quantification of dynamic contrast-enhanced (DCE) MRI and comparison with DCE-CT. Magn Reson Med 2011;66:1267–1274.
7. Heye T, Davenport MS, Horvath JJ, Feuerlein S, Breault SR, Bashir MR, Merkle EM, Boll DT. Reproducibility of dynamic contrast-enhanced MR imaging. Part I. Perfusion characteristics in the female pelvis by using multiple computer-aided diagnosis perfusion analysis solutions. Radiology 2013;266:801–811.

8. Ng CS, Raunig DL, Jackson EF, Ashton EA, Kelcz F, Kim KB, Kurzrock R, McShane TM. Reproducibility of perfusion parameters in dynamic contrast-enhanced MRI of lung and liver tumors: effect on estimates of patient sample size in clinical trials and on individual patient responses. AJR Am J Roentgenol 2010;194.
9. Schabel MC, DiBella EVR, Jensen RL, Salzman KL. A model-constrained Monte Carlo method for blind arterial input function estimation in dynamic contrast-enhanced MRI: II. In vivo results. Phys Med Biol 2010;55:4807–4823.
10. Kratochvíla J, Jiřík R, Bartoš M, Standara M, Starčuk Z, Taxt T. Distributed capillary adiabatic tissue homogeneity model in parametric multi-channel blind AIF estimation using DCE-MRI. Magn Reson Med 2016;75:1355–1365.
11. Zhang JL, Rusinek H, Bokacheva L, Chen Q, Storey P, Lee VS. Use of cardiac output to improve measurement of input function in quantitative dynamic contrast-enhanced MRI. J Magn Reson Imaging 2009; 30:656–665.
12. Parker GJM, Roberts C, Macdonald A, Buonaccorsi GA, Cheung S, Buckley DL, Jackson A, Watson Y, Davies K, Jayson GC. Experimentally-derived functional form for a population-averaged high-temporal-resolution arterial input function for dynamic contrast-enhanced MRI. Magn Reson Med 2006;56:993–1000.
13. Hittmair K, Gomiscek G, Langenberger K, Recht M, Imhof H, Kramer J. Method for the quantitative assessment of contrast agent uptake in dynamic contrast-enhanced MRI. Magn Reson Med 1994;31:567–571.
14. Schabel MC, Parker DL. Uncertainty and bias in contrast concentration measurements using spoiled gradient echo pulse sequences. Phys Med Biol 2008;53:2345–2373.
15. Garpebring A, Wirestam R, Östlund N, Karlsson M. Effects of inflow and radiofrequency spoiling on the arterial input function in dynamic contrast-enhanced MRI: a combined phantom and simulation study. Magn Reson Med 2011;65:1670–1679.
16. Cheng HLM, Wright GA. Rapid high-rsolution T1 mapping by variable flip angles: accurate and precise measurements in the presence of radiofrequency field inhomogeneity. Magn Reson Med 2006;55: 566–574.
17. Akbudak E, Conturo TE. Arterial input functions from MR phase imaging. Magn Reson Med 1996;36:809–815.
18. Fruytier AC, Magat J, Jordan B, Cron G, Colliez F, Gallez B. Erratum to dynamic contrast-enhanced MRI in mice at high field: estimation of the arterial input function can be achieved by phase imaging (Magn Reson Med 2014;71:544–550). Magn Reson Med 2014;72:602.
19. Beld E, Simonis F, Korporaal J, van der Heide U, Berg C Den. Automated correction method allowing phase-based detection of contrast enhancement in DCE-MRI. In Proceedings of the 22nd Annual Meeting of ISMRM, Milan, Italy, 2014. Abstract527.
20. Haacke EM, Brown RW, Thompson MR, Venkatesan R. Magnetic resonance imaging: physical principles and sequence design. New York: Wiley-Liss; 1999.
21. Williams DF, Wang CM, Arz U. In-phase/quadrature covariance-matrix representation of the uncertainty of vectors and complex numbers. 68th ARTFG Conf Dig 2006:62–65.
22. Brynolfsson P, Yu J, Wirestam R, Karlsson M, Garpebring A. Combining phase and magnitude information for contrast agent quantification in dynamic contrast-enhanced MRI using statistical modeling. Magn Reson Med 2015;74:1156–1164.
23. Van Osch MJ, Vonken EJ, Bakker CJ, Viergever MA. Correcting partial volume artifacts of the arterial input function in quantitative cerebral perfusion MRI. Magn Reson Med 2001;45:477–485.
24. Bruin PW de, Reijnierse M, van Osch MJ. Partial Volume correction of arteri al input functions in T1-weighted dynamic contrast-enhanced MRI. In Proceedings of the 18th Annual Meeting of ISMRM, Stockholm, Sweden, 2010. Abstract 1721.
25. Bernstein M, King K, Zhou X. Handbook of MRI pulse sequences. Amsterdam: Elsevier; 2004.
26. Donahue KM, Weisskoff RM, Burstein D. Water diffusion and exchange as they influence contrast enhancement. J Magn Reson Imaging 1997;7:102–110.
27. Cheng HLM. T1 measurement of flowing blood and arterial input function determination for quantitative 3D T1-weighted DCE-MRI. J Magn Reson Imaging 2007;25:1073–1078.
28. Hijnen NM, Elevelt A, Pikkemaat J, Bos C, Bartels LW, Grüll H. The magnetic susceptibility effect of gadolinium-based contrast agents on PRFS-based MR thermometry during thermal interventions. J Ther Ultrasound 2013;1:8.
29. Pintaske J, Martirosian P, Graf H, Erb G, Lodemann K-P, Claussen CD, Schick F. Relaxivity of Gadopentetate Dimeglumine (Magnevist), Gadobutrol (Gadovist), and Gadobenate Dimeglumine (MultiHance) in human blood plasma at 0.2, 1.5, and 3 Tesla. Invest Radiol 2006; 41:213–221.
30. Stanisz GJ, Odrobina EE, Pun J, Escaravage M, Graham SJ, Bronskill MJ, Henkelman RM. T1, T2 relaxation and magnetization transfer in tissue at 3T. Magn Reson Med 2005;54:507–512.
31. Pang Y, Bernardo M, Turkbey B, Ravizzini G, Thomasson D, Choyke P. Minimizing inflow effect in measured arterial input function for prostate DCE-MRI. In Proceedings of the 16th Annual Meeting of ISMRM, Toronto, Canada, 2008. Abstract 2775.
32. Lu H, Clingman C, Golay X, van Zijl PCM. Determining the longitudinal relaxation time (T1) of blood at 3.0 Tesla. Magn Reson Med 2004; 52:679–682.
33. Zhang X, Petersen ET, Ghariq E, De Vis JB, Webb AG, Teeuwisse WM, Hendrikse J, van Osch MJP. In vivo blood T 1 measurements at 1.5 T, 3 T, and 7 T. Magn Reson Med 2013;70:1082–1086.
34. Grgac K, Van Zijl PCM, Qin Q. Hematocrit and oxygenation dependence of blood 1H2O T1 at 7 tesla. Magn Reson Med 2013;70:1153–1159.
35. Cheng H-LM. Investigation and optimization of parameter accuracy in dynamic contrast-enhanced MRI. J Magn Reson Imaging 2008;28: 736–743.